

# Uranium Extraction with Cyanex272 Coated Magnetic Nanoparticles

Afshin Shahbazi<sup>1</sup>, Saeid Alamdar Milani<sup>1</sup>

1. Nuclear Fuel Cycle Research School, Nuclear Science and Technology Research Institute, AEOI, P.O.Box: 11365-8486, Tehran – Iran

## Abstract

In the Magnetically Assisted Chemical Separation (MACS) process, tiny ferromagnetic particles coated with solvent extractant are used to selectively separate radionuclides and hazardous metals from aqueous waste streams. The contaminant-loaded particles are then recovered from the waste solutions using a magnetic field. In the present study, Cyanex272 or C272 (bis (2,4,4-trimethylpentyl) phosphinic acid) coated magnetic particles are being evaluated for the possible application in the extraction of Uranium (VI) from nuclear waste streams. The uptake behaviour of U(VI) from nitric acid solutions was investigated by batch studies.

Adsorption of uranium (VI) from aqueous solution onto adsorbent was investigated in a batch system. Adsorption isotherm and adsorption kinetic studies of uranium (VI) onto nanoparticles coated Cyanex272 were carried out in a batch system. The factors influencing uranium (VI) adsorption were investigated and described in detail, as a function of the parameters such as initial pH value, contact time, adsorbent mass, and initial uranium (VI) concentration. Magnetically Assisted Chemical Separation (MACS) process adsorbent showed best results for the fast adsorption of U (VI) from aqueous solution at aqueous phase acidity value of 0.5 molar. In addition, more than 80% of U (VI) was removed within the first 2 hours, and the time required to achieve the adsorption equilibrium was only 140 minutes. Langmuir and Freundlich adsorption models were used for the mathematical description of the adsorption equilibrium. Equilibrium data agreed very well with the Langmuir model, with a maximum adsorption capacity of 48 mg.g<sup>-1</sup>. Adsorption kinetics data were tested using pseudo-first-order, pseudo-second-order and intra-particle diffusion models. Kinetic studies showed that the adsorption followed a pseudo-second-order kinetic model, indicating that the chemical adsorption was the rate-limiting step.

\*To whom correspondence should be addressed:  
salamdar@aeoi.org.ir

*Journal of Advanced  
Environmental  
Research and  
Technology*

Vol. 1, No.2  
page 3-19 ,spring 2023  
\*\*\*

Received 22 October 2022  
Accepted 25 January 2023

## key words

Uranium (VI) adsorption

MACS process

magnetic nanoparticles

Cyanex272



## 1. Introduction

Ion exchange and solvent extraction are two primary technologies currently being employed for the separation of transuranics and hazardous metal ions from waste solutions. These are complex processes that in some cases require expensive, bulky equipment and large chemical inventories. Further, they generate significant amounts of secondary waste. On the other hand, the Magnetically Assisted Chemical Separation (MACS) process provides a cost-effective way of removing transuranics from nuclear wastes [1,2].

The MACS process was developed at Argonne National Laboratory as a compact, simple process for selectively separating transuranics and fission product radionuclides from radioactive liquid waste streams. It employs small ferromagnetic composite particles coated with a selective solvent extractant or ion exchange material. The coated particles are mixed with the waste solution in situ or in a reactor vessel. The hazardous metals are selectively extracted onto the particle surface because of the chelating or exchange properties of the particle coating. The particles are removed by magnetic filtration or simply recovered with a magnet. The clean water can be reused by the facility or sent to sewerage. The target metals can be concentrated into a small volume by stripping the metals of the surface using an appropriate stripping agent. The concentrated product can be disposed properly, reused by the facility, or sent for resale and the MACS particles can be reused. There is an ongoing effort to evaluate the MACS process for the recovery of hazardous metals from industrial wastes for waste minimization and recycling efforts.

Uranium find extensive application as nuclear fuel in power plants and their main sources are soil, rocks, plants, sand and water [3]. Nuclear power is derived from uranium, which has no significant commercial use other than as a fuel for electricity generation.

In view of the extensive usage of uranium for various industrial purposes and potential risks presented by radionuclides for humans and the environment, precise determination of these metals in environmental, metallurgical, and geological materials is of greatest importance prior to pollution control measures or its use as alloys or in understanding the correlation between diseases of animals and aquatic organisms and soil chemistry. The most used methods for separation and

preconcentration of uranium include precipitation, co-precipitation, solvent extraction, membrane dialysis, chromatographic extraction, ion exchange, flotation and adsorption [4–11]. Most of these methods suffer from technical, economic and health problems related to selectivity, long time of extraction and large quantity of hazardous materials used.

Metals are extensively used in several industries, including mining, metallurgical, electronic,

electroplating and metal finishing. Uranium contamination of the environment from the mining and milling operations and nuclear waste disposal poses great threat to the environment. Contamination of groundwater resources by working and out of commission uranium mining operations is a well-known environmental problem. The harmful effects to the environment arises not only from the radioactive emissions from uranium series radionuclides, but also from the chemical toxicity of uranium [12, 13]. The United States Environment protection Agency (USEPA) has set the realistic regulation level of 30  $\mu\text{g/L}$  as the maximum contaminant level (MCL) for uranium [14]. The threat that the nuclear industry poses to the environment, especially from the leaching of U (VI) from uranium mine tailings to the groundwater is now viewed seriously. New stringent regulations have prompted the development of various technologies for its removal from wastewater produced from nuclear industries and mining activities. In oxidizing environments uranium occurs in the valence state +VI as the uranyl cation,  $\text{UO}_2^{2+}$ .

Adsorption using magnetic nanoparticles coated with a polymer is an important area of research. Grafting of new functional groups and chemical coated increases its adsorption capacity and selectivity towards metal ions in solution through the formation of different chelates [15]. A number of adsorbent materials are being investigated for the removal of U (VI) ions from aqueous solutions. They include Cyanex272, Cyanex932, chitosan, modified chitosan resins, cross linked poly 2,2-bisacrylamido acetic acid, phytic acid modified polyacrylamide–bentonite composite, chemically modified polyurethane foam and polymer grafted lignocelluloses [16-19]. The metal uptake by magnetic nanoparticles coated with Cyanex272 is primarily attributed to the phosphor and hydroxyl groups present in the polymer chain, which can interact with various metallic species through ion exchange and/or chelation mechanism.

Mechanisms responsible for Cyanex, although understood to a limited extent, may be one or combination of ion exchange, complexation, coordination, adsorption, electrostatic interaction, chelation and microprecipitation [20]. However, nanoparticles have several drawbacks. Nanoparticles are basically small particles, with low density, poor mechanical strength and little rigidity [21].

Magnetic nanoparticles are currently being widely studied and application of magnetic nanoparticle technology for remediating environmental problems has received attention in recent years [22-26]. It is believed that magnetic nanoparticles ( $\text{Fe}_3\text{O}_4$ ) show the finite-size effect and high ratio of surface-to-volume, resulting in a higher adsorption capacity [27]. Magnetic nano-carriers can be easily manipulated by an external magnetic field and hence should be suitable as the support of adsorbents. The super paramagnetic  $\text{Fe}_3\text{O}_4$  nanoparticles coated with polymers are usually composed of the magnetic cores to ensure a strong magnetic response and a polymeric shell to provide favourable functional groups and features. A composite of Cyanex272 with magnetic  $\text{Fe}_3\text{O}_4$  nanoparticles would result in an adsorbent with high binding capacity of metals [28].

In this work has combined magnetic nanoparticles into Cyanex272. The sorption process was studied with regard to the effects of aqueous phase acidity, initial uranium concentration, contact time, and dose of adsorbent. Equilibrium isotherms will be determined using Langmuir and Freundlich equations. The kinetics of the adsorption process will be analysed using pseudo-first-order, pseudo second-order and intra-particle diffusion models.

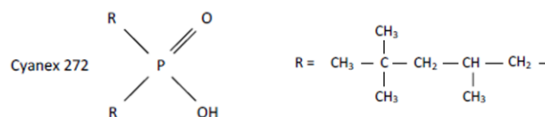
## 2. Materials and methods

### 2.1. Materials

Cyanex272, Iron (III) chloride hexahydrate ( $\text{FeCl}_3 \cdot 6\text{H}_2\text{O}$ ), iron (II) chloride tetrahydrate ( $\text{FeCl}_2 \cdot 4\text{H}_2\text{O}$ ), sodium hydroxide (NaOH), hydrochloric acid (HCl, 35wt.%), nitric acid ( $\text{HNO}_3$ , 63wt.%), polyethylene glycol-6000 (PEG-6000) and  $\text{UO}_2(\text{NO}_3)_2 \cdot 6\text{H}_2\text{O}$  (ACS grade) were purchased from Merck, Germany. pH of the working solutions was regulated by addition of  $\text{HNO}_3$  or NaOH solution. All the reagents used were of analytical-reagent grade and used as received. Ultrapure deionized water was obtained using the ELGA LabWater (UK) water purification system in our laboratory and was used to prepare all the solutions.

### 2.2. Reagent

Cyanex272 was kindly supplied by Cytec, Holland. The active component is bis (2,4,4-trimethylpentyl) phosphinic acid (M.W 290; density  $0.95\text{g cm}^{-3}$ ) having the following structure [29]:



### 2.3. Synthesis of Magnetite ( $\text{Fe}_3\text{O}_4$ ) nanoparticles and PEG-functionalized magnetite nanoparticles

The magnetic Nanoparticles (MNPs) were synthesized in aqueous solution using a modified version of the co-precipitation method. De-ionized water was de-aerated by sparging with nitrogen for 15 min. 4.4 gr of  $\text{FeCl}_3 \cdot 6\text{H}_2\text{O}$  and 1.98 gr of  $\text{FeCl}_2 \cdot 4\text{H}_2\text{O}$  were dissolved in 60 mL of the de-aerated water while the solution was continuously sparged with nitrogen (Airgas) to agitate the mixture and to prevent the oxidation of  $\text{Fe}^{2+}$  ions. After the complete dissolution of the iron compounds, sparging was maintained for an additional 30 minutes. The solution was then ultra-sonicated while the space above the solution was continuously purged with nitrogen. The mixture was stirred at  $70^\circ\text{C}$  until PEG 6000 added, then heated to  $265^\circ\text{C}$ , and refluxed for 30 min. The product was black. The black powder was collected with a permanent magnet, then redispersed in ethanol by supersonic for 15 min. The washing process was repeated three times. At last, the powder was dried at  $40^\circ\text{C}$  in vacuum.

### 2.4. Characterization of Magnetic Nanoparticles Coated cyanex272:

The newly formed cyanex272-magnetic nanoparticles beads obtained were confirmed by a Perkin-Elmer FT-IR System Model GX 55974 spectrometer.

cyanex272 (1.0 g) were added to 0.1 M hydrochloric acid (20 ml); the mixture was left to stand for 16 hours in a tightly closed bottle. The mixture was filtered, and the filtrate (5 ml) was titrated with a 0.1 M sodium hydroxide.

Then the samples were dried in vacuum at room temperature for 24 hours. After the process, the mixture was filtered, washed with distilled water and dried in vacuum at room temperature for 24 hours.



## 2.5. Batch experiments

Aliquot portions of uranium were placed in 25 mL high-density polypropylene bottles after the adjustment of pH to the desired value with dilute sodium hydroxide or nitric acid. MNPs adsorbent ( $5 \text{ g.L}^{-1}$ ) was added to each of the test solutions, and the sample bottles were then placed in a thermostated shaker (Infors AG, Aquatron). At different time intervals, the supernatant solutions were filtered, and the concentrations of uranium were determined by Inductively Coupled Plasma-Atomic Emission Spectroscopy (ICP-AES), spectrometer model 5500 Perkin-Elmer. The amount of uranium ion adsorbed was expressed in terms of the distribution coefficient. For isotherm studies, a series of test tubes were used. Each test tube was filled with 25 mL of each ion solution of varying concentrations and a known dose of adsorbent ( $5 \text{ g.L}^{-1}$ ) was added into each test tube and agitated for a specific period. The metal ion concentration retained in the adsorbent ( $\text{mg.g}^{-1}$ ) was calculated by:

### 3.1.1. X-ray power diffraction

Fig. 1. shows the XRD pattern of the sample, which is quite identical to pure magnetite and matched well with that of it, indicating that the sample has a cubic crystal system. Also, we can see that no characteristic peaks of impurities were observed.

The mean particle diameters were also calculated from the XRD pattern according to the line width of the plane refraction peak using Scherrer Eq. (2):

$$D_c = K\lambda / (b \cdot \cos[\theta]) \quad (2)$$

The equation uses the reference peak width at angle  $\theta$ , where  $\lambda$  is the X-ray wave length,  $b$  is the width of the XRD peak at half height and  $K$  is a shape factor, about 0.89 for magnetite.

The crystal structures of as-synthesized MNPs and MNPs-PEG were characterized by XRD and the results are presented in Fig. 1. and 2. The XRD patterns show the characteristic peaks for  $\text{Fe}_3\text{O}_4$  at 30.1 (220), 35.5 (311), 43.1 (400), 53.4 (422), 57.0

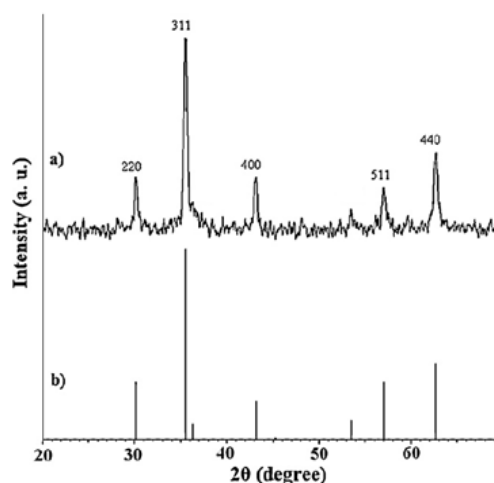


Fig. 1. the XRD pattern of pure nanoparticles (b) and pure synthesized magnetic nano particles

$$q_e = (C_i - C_e) \times V/m \quad (1)$$

Where  $C_0$  and  $C_e$  are the initial and equilibrium concentrations of the ion(s) ( $\text{mg.L}^{-1}$ ), respectively,  $V$  is the volume of the aqueous solutions (mL), and  $m$  is the weight of the sorbent used (g). To evaluate the nature of adsorption, the experimental data were analyzed with the Freundlich and Langmuir models.

## 3. Results and Discussion

### 3.1. Physicochemical characterization

(511) and 62.6 (440), which are in agreement with the database in JCPDS file (PCPDFWIN v.2.02, PDF No. 85-1436). The diffraction peaks reveal that the MNPs are pure  $\text{Fe}_3\text{O}_4$  with a spinel structure (Fig. 1). Also Fig. 2. shows XRD result of MNPs-PEG and that their size is 19 nm.

### 3.1.2. FT-TR spectra of $\text{Fe}_3\text{O}_4$ nanoparticles with PEG

The presence of PEG layer on nanoparticle surface was more characterized by FT-IR spectroscopy as shown in Fig. 3. FT-IR spectra of PEG-6000 and unmodified nanoparticles are demonstrated in Fig. 3a and c for comparison. The -C-O-C- ether



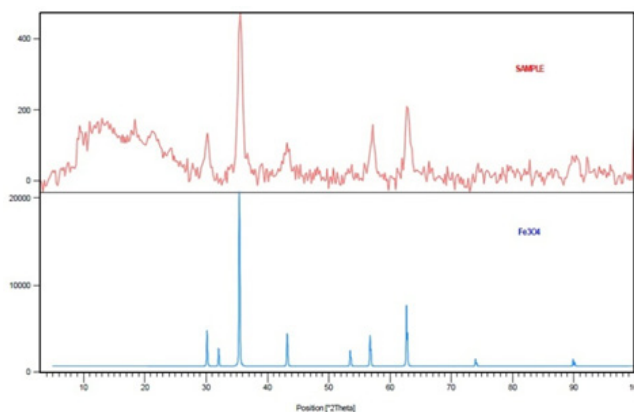


Fig. 2. the XRD pattern of nanoparticles with coated PEG (below) and coated PEG synthesized magnetic nanoparticles

stretch band and the vibration band (antisymmetric stretch) are appeared in PEG spectrum at  $1101.1\text{ cm}^{-1}$  and  $1349.4\text{ cm}^{-1}$ , respectively (Gupta and Wells, 2004). Besides, the absorption bands of  $1281.3\text{ cm}^{-1}$  and  $1468.8\text{ cm}^{-1}$  attribute to the vibration of  $-\text{CH}_2$  (Hu et al., 2008) and that around  $953.2\text{ cm}^{-1}$  corresponds to  $-\text{CH}$  out-of-plane bending vibration. The transmittance band at  $578.1\text{ cm}^{-1}$  of Fig. 3c is the stretching mode of Fe-O in  $\text{Fe}_3\text{O}_4$  (Ahmadi et al., 2011). The broad peak near  $3450\text{ cm}^{-1}$  in both spectra of PEG and iron oxide belongs to attached hydroxyl groups (Gupta and Wells, 2004). The PEG modified nanoparticle spectrum in Fig. 3b comprises the main absorbance of ether stretch band at the  $1104.6\text{ cm}^{-1}$  and  $-\text{CH}_2$  vibrational band at  $1260.8\text{ cm}^{-1}$  and  $1411.5\text{ cm}^{-1}$ . This spectrum verifies that PEG can be found on the surface of synthesized nanoparticles. However, the characteristic absorbance peaks show a small shift to lower frequencies due to changing the environment of PEG added layer [30]. Effective chemical bonding likely leads to such a phenomenon [31, 32]. Similarly, shift of Fe-O vibration of coated nanoparticles to  $598.2\text{ cm}^{-1}$  suggests the

new band formation between iron oxide surface and PEG coating [33].

### 3.1.3. FT-TR spectra of $\text{Fe}_3\text{O}_4$ nanoparticles coated Cyanex272

The FT-IR spectra of Cyanex 272 and its sodium salt synthesized in laboratory were analysed and compared (Fig. 4 and 5). The FT-IR spectra of Cyanex 272 show bands corresponding to vibrations of phosphinic moiety: the P=O stretching bands at  $1170\text{ cm}^{-1}$  and the P-OH band at  $1048\text{ cm}^{-1}$ . The O-H moiety gives the broad bands at  $3351$ ,  $2699$  and  $2294\text{ cm}^{-1}$  corresponding to the bonded O-H vibrations and the broad band at  $1695\text{ cm}^{-1}$  representing O-H deformation vibrations. The spectrum also shows a strong band at  $960\text{ cm}^{-1}$  which is assigned to the P-O-H group.

### 3.2. Effect of $\text{HNO}_3$ concentration Variation on the uptake of U (VI) with Cyanex272-coated magnetic particles

The  $\text{HNO}_3$  concentration variations effect on the adsorption of uranium (VI) onto Cyanex272 coated magnetic nanoparticles was investigated using  $50\text{ mg.L}^{-1}$  of uranium (VI) concentration for an

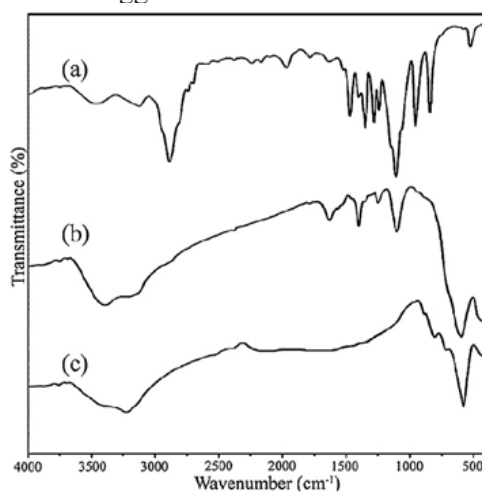


Fig. 3. FTIR spectrum of (a) PEG-10000, (b) PEG-coated and (c) bare iron oxide nanoparticles.

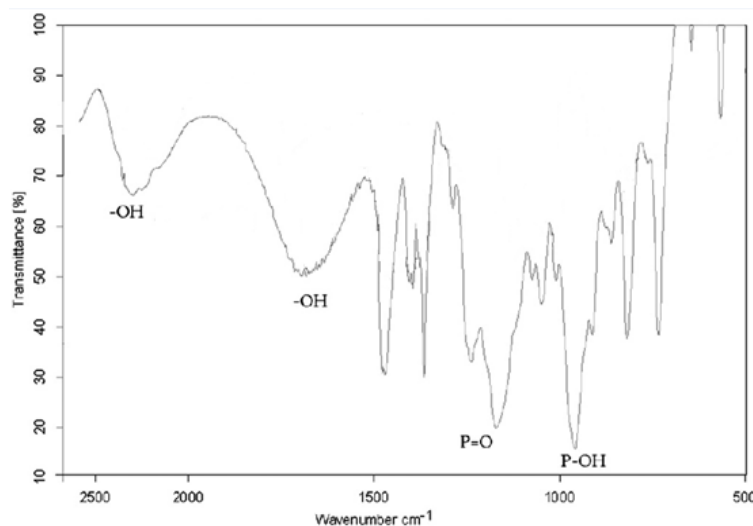


Fig. 4. FT-IR spectra of the organic phase of Cyanex 272.

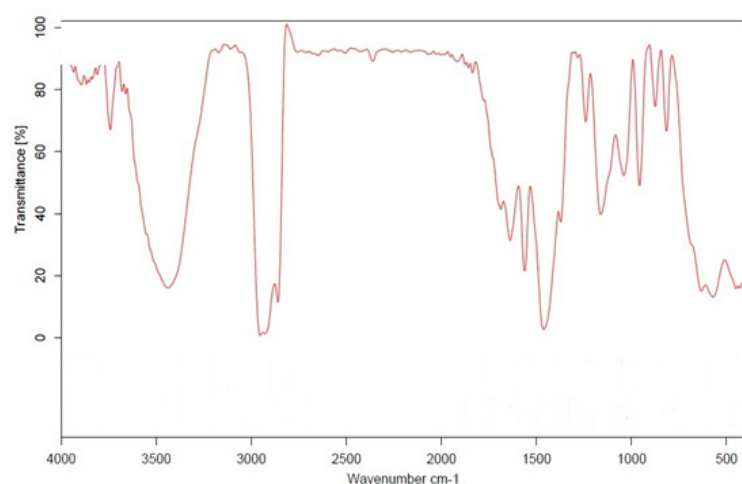
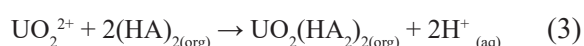


Fig.5. FT-IR spectra of the nanoparticles coated Cyanex272

aqueous phase acidity range of 0.1 to 5 molar at 25°C for 180 min. The results are shown in Fig. 6. The uranium (VI) removal efficiency was strongly depended on pH of the solution. The removal efficiency decreased with increasing HNO<sub>3</sub> concentration to a maximum value (0.5 M) and then declines slowly. The efficiency remains up to 87% with further increase up to 0.5 M. Hence it has a good adsorption capability in the range of 0.1 to 0.5. The removal efficiency of U (VI) decreases remarkably with increasing HNO<sub>3</sub> concentration.



Where HA is Cyanex272.

In strong acidic solutions (less than 0.5M), more protons will be able to protonate amine groups to form  $-\text{NH}_3^+$  groups on the Cyanex272 surface, reducing the number of binding sites for the adsorp-

tion of  $\text{UO}_2^{2+}$  due to electrostatic repulsion, as a result, the removal efficiency of uranium decreases a little in strong acidic solutions (less than 0.5M). The hydrolysis of uranyl ions plays important role in determining the equilibrium between uranium (VI) in solution and on adsorbent. The products of hydrolysis includes  $\text{UO}_2(\text{OH})^+$ ,  $(\text{UO}_2)_2(\text{OH})_2^{2+}$ ,  $(\text{UO}_2)_3(\text{OH})_5^{3+}$ ,  $(\text{UO}_2)_2(\text{OH})_2$ , which results in decline of adsorption removal efficiency of uranium (VI). It can be explained that pH plays an important role in dissociating proton of functional groups, resulting in more negatively charged functional groups, and the capacity of combination between functional groups and U (VI) can also be enhanced. However, when the aqueous phase acidity is higher than a certain value, (greater than 0.5 M)  $\text{OH}^-$  itself has a tendency to combine with U (VI), and it competes with functional groups on the adsorbent for metal ions, leading to the decrease of the adsorption capacity [34]. The optimal HNO<sub>3</sub>

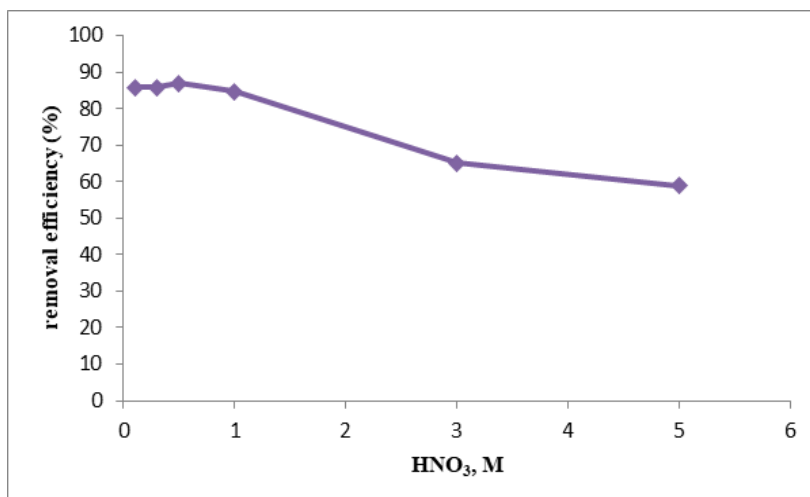


Fig. 6. Effect of the HNO<sub>3</sub> concentration variations on the adsorption of uranium (VI) ([UO<sub>2</sub><sup>2+</sup>] = 50 mg/L, adsorbents = 5mg, and T=25°C).

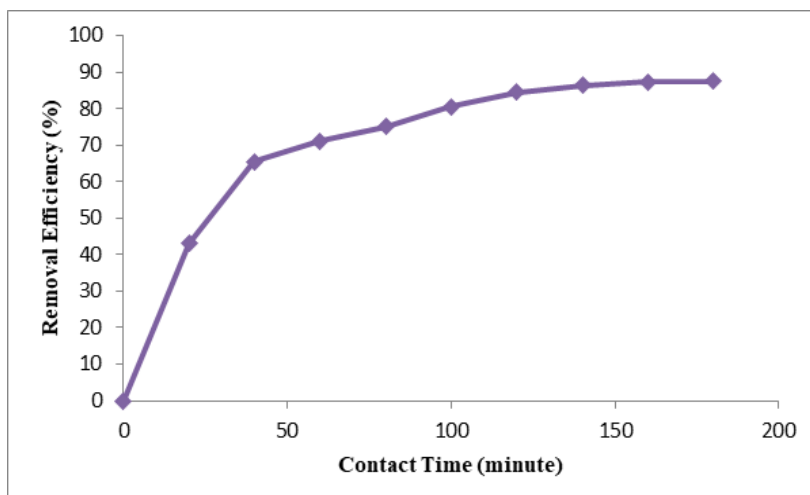


Fig. 7. Effect of contact time on the adsorption of uranium (VI) ([UO<sub>2</sub><sup>2+</sup>] = 50 mg/L, 5 mg.L<sup>-1</sup> dose of adsorbent, 0.5 M HNO<sub>3</sub>, and T=25°C).

concentration of 0.5 M was selected for further study in the other experiments.

### 3.3. Effect of Contact Time on the uptake of U (VI) with Cyanex272-coated magnetic particles

Equilibrium time is another important parameter to uranium (VI) adsorption. Under the conditions of 5 mg.L<sup>-1</sup> dose of adsorbent, 0.5 M HNO<sub>3</sub>, room temperature and 50 mg/L uranium (VI), the adsorption experiments were carried out for contact time varied from 20 to 180 minutes (20, 40, 60, 80, 100, 120, 140, 160, 180). The results are shown in Fig. 7.

The adsorption capacity of uranium (VI) onto Cyanex272-Magnetic Nano Particles (C272-MNPs) increases with an increase of contact

time, and reaches adsorption equilibrium within 140 minutes. Adsorption kinetics of uranium (VI) consisted of two phases: first rapid phase where adsorption was fast and contributes significantly to equilibrium uptake, and a slower second phase whose contribution to the total metal adsorption was rather small. The maximum removal capacity was achieved at around 140 min, with removal percentage of 87%. After 140 minutes, the change of adsorption capacities for uranium (VI) did not show noteworthy effects. As a result, the adsorption equilibrium time considered as 140 minutes. The C272-MNPs adsorbent showed best adsorption of U (VI) in the time range. Such a fast adsorption rate could be attributed to the functional groups on adsorbent. Some literatures for exam-

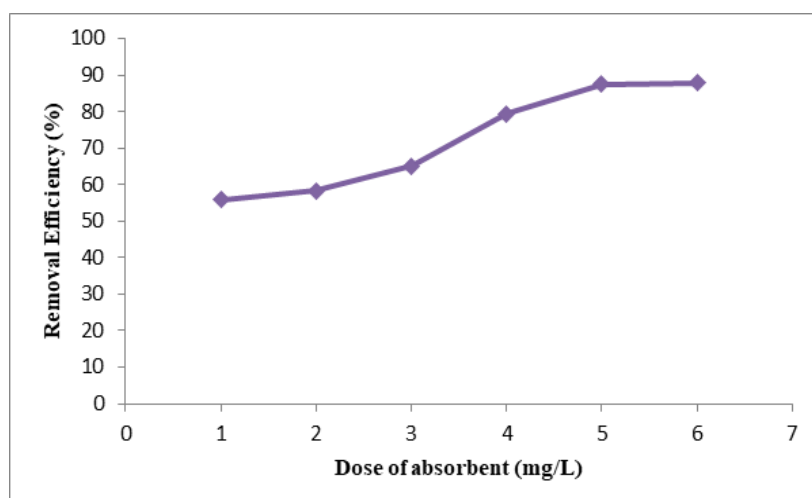


Fig. 8. The adsorption removal efficiency for variable dose of adsorbent, uranium (VI) ( $[UO_2^{2+}]$  at 50 mg/L, at 0.5 M  $HNO_3$  and  $T=25^\circ C$ , 140 min).

ple; [35-39], have reported Uranium (VI) adsorption on the cross-linked chitosan took about 180 min to reach the maximum adsorption. In a review by [40] the removal of some metal ion such as Hg, Cu, Ni, Zn, Pb and Mn by chitin and chitosan-derivatives showed a similar trend of maximum adsorption time of 120-180 min. From the Fig. 7. it shows that the rate of U (VI) adsorption becomes slower at later stages. It may be attributing to the great decrease of the bonding sites on the surface of C272-MNPs and the aggregation between particulates and saturation of adsorbent.

### 3.4. Effect of Adsorbents Dose on the uptake of U (VI) with Cyanex272-coated magnetic particles

The effect of adsorbents concentration on the adsorption removal efficiency was studied by contacting a variety of adsorbent dose (1, 2, 3, 4, 5 and 6  $mg.L^{-1}$ ) at a constant temperature ( $25^\circ C$ ) and 0.5 M  $HNO_3$  using 50  $mg.L^{-1}$  of uranium (VI) concentration for 140 min. The results are shown in Fig. 8. The removal efficiency of uranium (VI) increased with increasing adsorbents concentration in the aqueous solution. The adsorption surface area gets larger with increasing of the mass of the adsorbents. C272-MNPs adsorbent showed greatest results, even at the lowest concentration ( $1 mg.L^{-1}$ ), the removal efficiency was more than 55%. The efficiency increases up to 87% when the concentration of the adsorbent is 5  $mg.L^{-1}$ .

### 3.5. Effect of Uranium (VI) Concentration on the uptake of U (VI) with Cyanex272-coated magnetic particles

The effect of uranium (VI) concentration on the

adsorption removal efficiency was studied by contacting a fixed dose of adsorbent ( $5 mg.L^{-1}$ ) for 140 minutes at a fixed temperature ( $25^\circ C$ ) and 0.5 M  $HNO_3$  using a variety of uranium (VI) concentrations (10, 20, 30, 40, 50, 60, 70, 80, 90, 100, 110, 120, 130 and 140  $mg.L^{-1}$ ). The results are shown in Fig. 9 and 10.

The removal efficiency of uranium (VI) decreased from 87 to 60% with increasing uranium (VI) concentration in the aqueous solution. This phenomenon can be explained since adding more mass of uranium into the system will increase the initial uranium (VI) concentration in the aqueous solution, but the amount of the adsorbent remains the same. The adsorption capacity  $Q$ , was calculated based on the difference of uranium concentration before and after adsorption. The adsorption capacity of adsorbents for uranium increased with increase of uranium concentration, as the amount of the adsorbent remains unchanged. This result is similar to that reported by Kutahyal and Eral, (2004) [41] in their study on selective adsorption of uranium from aqueous solutions using activated carbon prepared from charcoal by chemical activation. From the Fig. 9., it can be deduced that the maximum adsorption capacity for U (VI) was about 48 mg per gram adsorbent at uranium concentration. This gives a removal efficiency of 87%.

Hudson and Matejka [42] applied polymeric microspheres for heavy metal adsorption, and found that the adsorption capacities were just between 14.4 and 24.6 mg/g Erdal et al. [43] used polyethyleneglycol-methacrylate (PEGMA)-co-vinylimidazole (VI) microspheres as adsorbents and found that its adsorption capacity was only 25 mg/g for



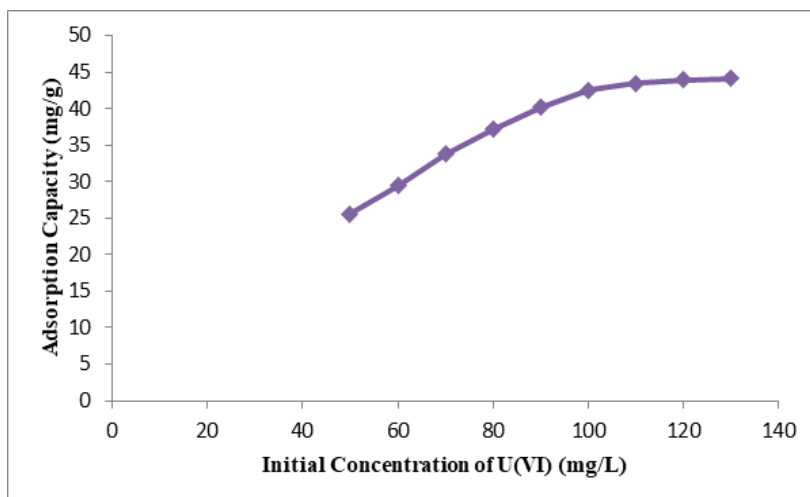


Fig. 9. The adsorption capacity under variable uranium (VI) concentration; 5 mg adsorbent amount, 0.5 M HNO<sub>3</sub>, and T=25°C, 140 min).

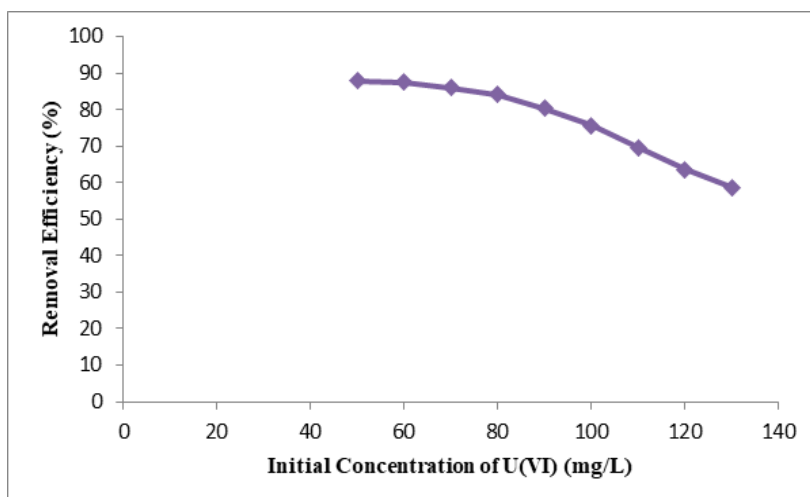


Fig. 10. The adsorption removal efficiency under variable uranium (VI) concentration adsorbents; 10 mg adsorbent amount, 0.5M HNO<sub>3</sub>, and T = 25°C).

heavy metals. Compared with the data mentioned above, the C272-MNPs performs better in the treatment of U (VI) in solution. It can be further indicated that the C272-MNPs has a good potential as adsorbent for the treatment of other metals.

#### 4. Kinetic studies

The mechanism of adsorption depends on the physical and/or chemical characteristics of the adsorbent as well as on the mass transport process. In order to determine the mechanism of U (VI) adsorbed onto C272-MNPs, several commonly used adsorption kinetic models were employed to discuss the controlling mechanism [44-46].

Several kinetic models such as pseudo-first-or-

der, pseudosecond- order and intra-particle diffusion model have been applied to find out the adsorption mechanism. The equation of the two kinetic models is expressed as follows.

The pseudo first-order model of Lagergren is based on the assumption that the rate of change of adsorbed solute with time is proportional to the difference in equilibrium adsorption capacity and the adsorbed amount [44, 47]. The pseudo first-order equation is expressed as follows [48]:

$$dq/dt = K(q_e - q_t) \quad (4)$$

When the boundary conditions  $qt = 0$  at  $t = 0$ , Eq. (4) can be integrated into the following equation



[49]:

$$\log (q_c - q_t) = \log q_c - (K/2.303) t \quad (5)$$

Where  $q_e$  and  $q_t$  are the adsorption capacity per unit weight of adsorbent at equilibrium and at time  $t$  (h), respectively ( $\text{mg.g}^{-1}$ ), and  $K$  is the pseudo first-order rate constant ( $\text{h}^{-1}$ ). The linearized form of the pseudo-first order model for the sorption of U (VI) ions onto C272-MNPs is given in Fig. 11. The linear plot of  $\log(q_e - q_t)$  against time ' $t$ ' demonstrates the applicability of the above equation for U (VI) ions sorption onto C272-MNPs. The rate constant  $K = 0.0393 \text{ h}^{-1}$  was calculated from the slope of the straight line with a correlation factor of 0.8824. It is found that a correlation coefficient value is low, showing the bad quality of linearization. Additionally, the  $q_e$  value acquired by this method is contrasted with the experimental value. So the reaction cannot be classified as first-order. One suggestion for the differences in experimental and theoretical  $q_e$  values is that there is a time lag, possibly due to a boundary layer or external resistance controlling at the beginning of the sorption. This time lag is also difficult to quantify. For this reason, it is necessary to use a trial and error method in order to obtain the equilibrium uptake [50].

The pseudo second-order model is based on the assumption that the rate-limiting step involves chemisorption [44, 48]. The equation is represented as follows [51]:

$$dq_t/dt = K (q_c - q_t)^2 \quad (6)$$

When the initial conditions  $q_t = 0$  at  $t = 0$ , after integration, the linear form of the pseudo-second-order equation is given [51]:

$$t/q_t = 1/(K.q_c^2) + t/q_c \quad (7)$$

Where  $K$  is the second-order adsorption rate constant ( $\text{g.mg}^{-1}.\text{h}^{-1}$ ), and  $q_e$  is the adsorption capacity calculated by the pseudo-second order kinetic model ( $\text{mg.g}^{-1}$ ). The rate constant was calculated from the slope of the straight line (Fig. 12). The rate constant was calculated from the slope of the straight line (Fig. 12). The rate constant  $K = 0.0007 \text{ h}^{-1}.\text{mg}^{-1}$  was calculated from the slope of the straight line with a correlation factor of 0.991.

Besides, the calculated  $q_t$  values agreed very well with the experimental data. Thus experiment results supports the assumption behind the model that the rate limiting step in adsorption of U (VI) is chemisorption involving valence forces through the sharing or exchange of electrons between adsorbent and metal ions. Some studies on the kinetics of U (VI) adsorption onto various adsorbents have also reported higher correlations for pseudo-second order model [52, 53]. Also it was found that the kinetics of adsorption from a solution onto an adsorbent theoretically, and the adsorption process obeyed first-order kinetics at high initial concentration of solution while it obeyed pseudo-second-order kinetics at lower initial concentration of solution [54, 55].

The intra-particle diffusion model is used to explain diffusion mechanism of adsorption process [56]. The intra-particle diffusion model can be described as follows [57]:

$$q_t = K_{id} (t)^{0.5} + C \quad (8)$$

Where  $K_{id}$  is the intra-particle diffusion rate constant ( $\text{mg.g}^{-1}.\text{h}^{-0.5}$ ) and  $C$  is the intercept. The value of  $C$  relates to the thickness of the boundary layer. The larger  $C$  implies the greater effect of the boundary layer. According to Eq. (8), if adsorption mechanism follows the intra-particle diffusion model, the plot of  $q_t$  against  $t^{0.5}$  should show linear relationship. Slope  $K_{id}$  and intercept  $C$  will be obtained by linear fitting analysis. The plot of  $q_t$  versus  $t^{0.5}$  is given in Fig. 13. The value of rate constant of Morris–Weber transport,  $K_{id}$ , calculated from the slope of the linear plot are shown in Fig. 13. The rate constant  $K_{id} = 1.781 \text{ mg.g}^{-1}.\text{h}^{-0.5}$  was calculated from the slope of the straight line with a correlation factor of 0.9881. As can be seen, the adsorption process was controlled by pseudo-second-order equation and the intra-particle diffusion model. The correlation coefficient of the intra-particle diffusion equation is lower than the pseudo-second-order equation. It could be interpreted as follows: firstly, the removal of U (VI) from aqueous solution cannot be neglected relative to the amount of U (VI) in the solution; secondly, the intra-particle diffusivity relies on the solid phase concentration in a large degree [58, 59]. Due to the two reasons, the correlation coefficient of the intra-particle diffusion equation is not suitable.

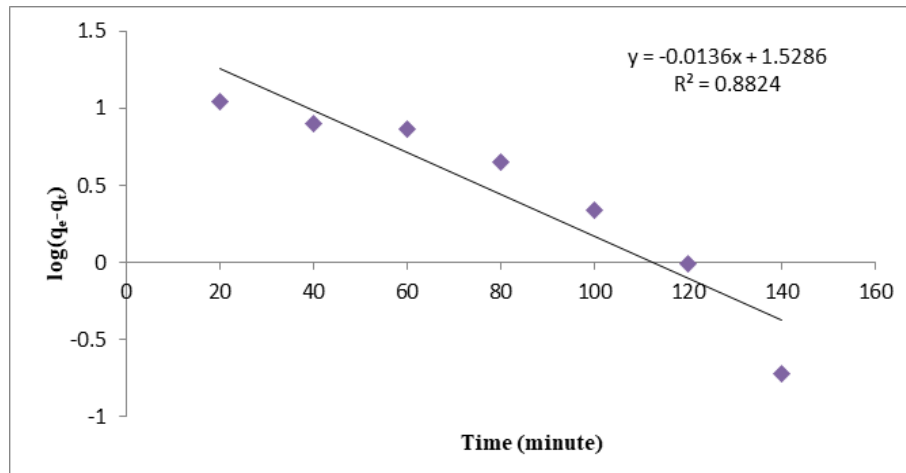


Fig. 11. the first order kinetic plot of U (VI) adsorption on C272-MNPs (the initial concentration,  $\text{HNO}_3$  concentration, volume of solution and amount of adsorbent was  $50 \text{ mg.L}^{-1}$ ,  $0.5 \text{ M}$ ,  $25 \text{ ml}$  and  $5 \text{ g.L}^{-1}$  respectively).

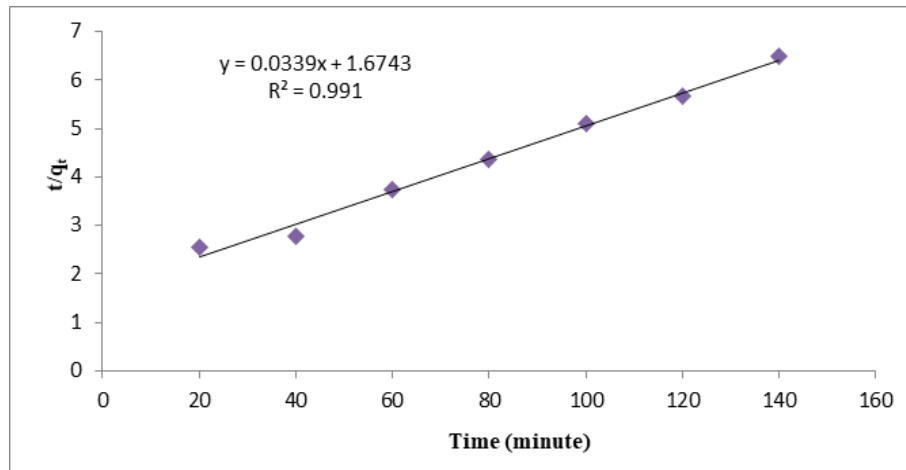


Fig. 12. the Pseudo second order kinetic plot of U (VI) adsorption on C272-MNPs (the initial concentration,  $\text{HNO}_3$  concentration, volume of solution and amount of adsorbent was  $50 \text{ mg.L}^{-1}$ ,  $0.5 \text{ M}$ ,  $25 \text{ ml}$  and  $5 \text{ g.L}^{-1}$  respectively).

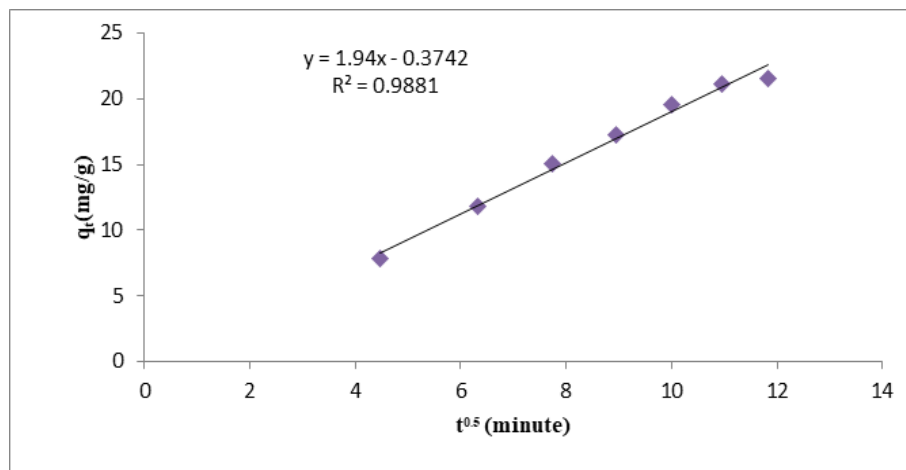


Fig. 13. Intraparticle plot of U (VI) adsorption on C272-MNPs (the initial concentration,  $\text{HNO}_3$  concentration, volume of solution and amount of adsorbent was  $50 \text{ mg.L}^{-1}$ ,  $0.5 \text{ M}$ ,  $25 \text{ ml}$  and  $5 \text{ g.L}^{-1}$  respectively).



## 5. Adsorption Isotherms

The adsorption isotherm is fundamental information, which specifies how the adsorbent molecules distribute between the liquid and the solid phase when the adsorption process reaches an equilibrium state. Using the data from the adsorption experiments conducted in a series of U (VI) solutions with different initial concentrations, the adsorption capacity and adsorption behavior of U (VI) were analyzed by adsorption isotherm. Fig. 14. shows the adsorption isotherm of uranium (VI) on the C272-MNPs.

The Langmuir and Freundlich models are usually used to describe equilibrium adsorption isotherms.

$$C_e/q_e = 1/(Q_0 \cdot b) + C_e/Q_0 \quad (9)$$

Where  $b$  is a constant of adsorption equilibrium ( $L \cdot mg^{-1}$ ), and  $Q_0$  is the saturated monolayer adsorption capacity ( $mg \cdot g^{-1}$ ). A linearized plot of  $C_e/q_e$  against  $C_e$  gives a  $Q_0$  and  $b$ . The plot of specific sorption,  $C_e/q_e$ , against the equilibrium concentration,  $C_e$  for C272-MNPs is shown in Fig. 14.

An alternate isotherm based on adsorption on a heterogeneous surface developed by Herbert F. Freundlich is Freundlich isotherm (Mellash and Chegrouche, 1997). In 1909, Freundlich gave an empirical expression representing the variation of isothermal adsorption of gas, adsorbed by unit

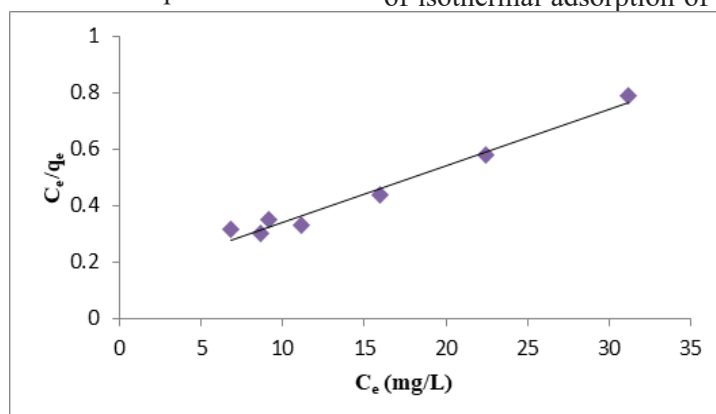


Fig. 14. Adsorption isotherm of uranium (VI) on C272-MNP, plotted according to the linearized Langmuir equation.

The amount of adsorption at equilibrium time  $t$ ,  $q_e$  ( $mg/g$ ), was calculated as mentioned previously. The Langmuir isotherm considers the adsorbent surface as homogeneous and all adsorption sites equivalent. There is no interaction between adsorbed molecules and at the maximum adsorption, only a monolayer of adsorbate is formed on the surface of the adsorbent. The Eq. (9) represents the Langmuir isotherm:

mass of solid adsorbent with pressure. The empirical Freundlich equation based on adsorption on a heterogeneous surface (Eq. 10) is given as follows: (Mellash and Chegrouche 1997):

$$q_e = K_F \times C_e^{1/n} \quad (10)$$

This expression can be linearized to give (Eq. 11), which is:

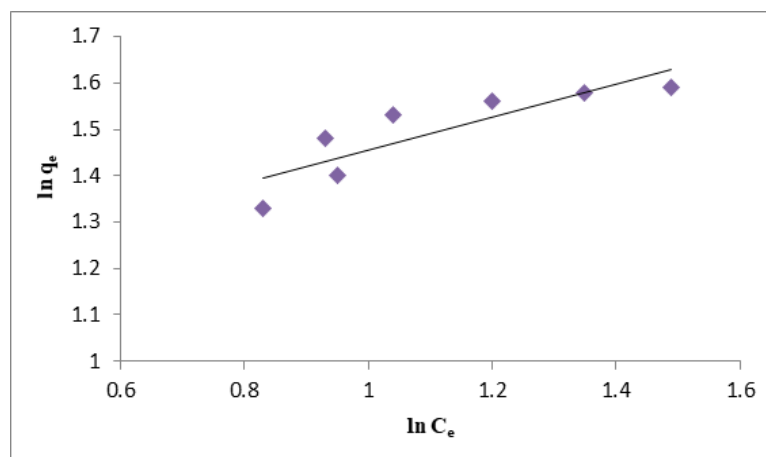


Fig. 15. Adsorption isotherm of uranium (VI) on C272-MNP, plotted according to Freundlich equation.

$$\ln q_e = \ln K_F + \ln C_e \quad (11)$$

Where  $K_F$  and  $n$  are Freundlich constants, which represent adsorption capacity and adsorption intensity, respectively.  $K_F$  and  $n$  was determined from a linear plot of  $\ln q_e$  against  $\ln C_e$  (Fig. 15). The calculated results of the Langmuir and Freundlich isotherm constants are given in Table 1.

It is found that the adsorption of uranium (VI) on

Table 1 Langmuir, Freundlich isotherm model constants and correlation coefficients.

Freundlich model		
$K_F$ (mg/g)	$n$	$R^2$
12.67	2.84	0.752
Langmuir model		
$Q_0$ (mg/g)	$b$ (L/mg)	$R^2$
48.32	0.14	0.977

the C272-MNPs correlated well ( $R > 0.97$ ) with the Langmuir equation as compared the Freundlich equation under the concentration range studied. The Langmuir isotherm considers the adsorbent surface as homogeneous and all adsorption sites equivalent. There is no interaction between adsorbed molecules and at the maximum adsorption, only a monolayer of adsorbate is formed on the surface of the adsorbent. Langmuir model is suitable for adsorption equilibrium of uranium (VI) onto C272-MNPs with a maximum adsorption capacity of 48 mg/g at 25°C.

The essential characteristics of the Langmuir isotherm can be expressed in terms of dimensionless constant separation factor,  $R_L$  which is used to predict if an adsorption system is preferable or not. The separation factor,  $R_L$  is given by (Bhatnagar and Jain, 2005) (Eq. 12):

$$R_L = 1/(1 + (b.C_0)) \quad (12)$$

Where  $C_0$  is the initial uranium (VI) concentration ( $\text{mg.L}^{-1}$ ) and  $b$  is the Langmuir adsorption constant ( $\text{L.mg}^{-1}$ ).

Based on the effect of separation factor on isotherm shape, the  $R_L$  values are in the range of  $0 < R_L < 1$ . The calculated  $R_L$  values, ranging from 0.0521 to 0.1250 for different initial U (VI) concentrations, indicated that adsorption of U (VI) by C272-MNPs was favorable [58-61].

## 6. Conclusion

In this work, C272-MNPs was synthesized and characterized as a new adsorbent for U (VI) ad-

Table 2  $R_L$  values based on the Langmuir equation.

Initial uranium (VI) concentration (mg/L)	$R_L$ Value
50	0.1250
60	0.1064
70	0.0926
80	0.0820
90	0.0735
100	0.0667
110	0.0610
120	0.0562
130	0.0521





sorption from aqueous solution. The adsorbent was prepared on the surface of Cyanex272-coated magnetic nanoparticles. The batch adsorption experiments have proven that the removal efficiency of U (VI) adsorbed by C272-MNPs was enhanced on the surface of Cyanex272-coated magnetic nanoparticles. The C272-MNPs was shown to be efficient adsorbent for the adsorption of U (VI) from aqueous solution at  $\text{HNO}_3$  concentration values from 0.1 to 5 M  $\text{HNO}_3$ , with maximum adsorption removal efficiency at 0.5 M. In addition, more than 85% of U (VI) ions were removed by 5 mg of C272 -MNPs within the first 2 hours, and the time required to achieve the adsorption equilibrium was only 140 minutes.

Magnetic nanoparticles were synthesized rapidly. The application of magnetic nanoparticles in extraction processes allows fast and cost effective extraction from the reaction mixture without filtration or centrifugation, therefore representing a gentle, versatile, scalable, and easy to automate separation process.

The adsorption dynamic results showed that the adsorption process obeys a Langmuir adsorption isotherm. C272-MNPs adsorbent is not only effective sorbent of uranium, but also it is cost effective and environmentally friendly. The usage of magnetic nanoparticles reduces the energy costs.



## References

1. Milani S.A. , Darban A.K., Shahbazi A, 2015, Synthesis and characterization of cyanex 272-modified superparamagnetic magnetite nanoparticles, *Journal of Nuclear Science and Technology* 2015 , volume - , Number 70; Page(s) 64 To 76.
2. M.D. Kaminski, L. Nunez, *Sep. Sci. Technol.* 37 (2002) 3703.
3. V.K. Jain, R.A. Pandya, S.G. Pillai, P.S. Shrivastav, Simultaneous preconcentration of uranium(VI) and thorium(IV) from aqueous solutions using a chelating calix[4] arene anchored chloromethylated, *Talanta* 70 (2006) 257–266.
4. F.A. Aydin, M. Soylak, A novel multi-element coprecipitation technique for separation and enrichment of metal ions in environmental samples, *Talanta* 73 (2007) 141–147.
5. Y.K. Agrawal, P. Shrivastav, S.K. Mnom, Solvent extraction separation of uranium (VI) with crown ether, *Sep. Purif. Technol.* 20 (2000) 177–183.
6. A.T. Kuhu, *Electrochemistry of Cleaner Environments*, Plenum Press, New York, 1972.
7. M.L. Dietz, H.E. Philip, L.R. Sajdak, R. Chiari- zia, An improved extraction chromatographic resin for the separation of uranium from acidic nitrate media, *Talanta* 54 (2000) 1173–1184.
8. A.C. Ladeira, C.A. Morais, Uranium recovery from industrial effluent by ion exchange-column experiments, *Miner. Eng.* 18 (2005) 1337–1340.
9. T.P. Rao, P. Metilda, J.M. Gladis, Preconcentration techniques for uranium (VI) and thorium (IV) prior to analytical determination, *Talanta* 68 (2006) 1047–1064.
10. A.M. Donia, A.A. Atia, E.M. Moussa, A.M. El-Sherif, M.O. Abd El-Magied, Removal of uranium (VI) from aqueous solutions using glycidyl methacrylate chelating resins, *Hydromet.* 95 (2009) 183–189.
11. Y. Jung, S. Kim, S. Park, J.M. Kim, Application of polymer modified nanoporous silica to adsorbents of uranyl ions, *Colloids. Surf. A* 31 (2008) 162–166.
12. Bargar, J.R., R. Reitmeyer, J.A. Davis, 1999. Spectroscopic confirmation of uranium(VI) – carbonato adsorption complexes on hematite. *Geochimica et Cosmochimica Acta*, 33: 2481-2484.
13. Bargar, J.R., R. Reitmeyer, J.J. Lenhart, J.A. Davis, 2000. Characterization of uranium(VI) - carbonato complexes on hematite: EXAFS and electrophoretic mobility measurements. *Geochimica et Cosmochimica Acta*, 64: 2737-2749.
14. Reimann, C., D. Banks, 2004. Setting action levels for drinking water: are we protecting our health or our economy (or our backs!)? *Sci. Total Environ.*, 332: 13-21.
15. Anirudhan, T.S., C.D. Bribble, S. Rijith, 2010. Removal of uranium(VI) from aqueous solutions and nuclear industry effluents using humic acid-immobilized zirconium-pillared clay. *J. Environ. Radioact.*, 101: 267-276
16. Anirudhan, T.S. and P.G. Radhakrishnan, 2009. Improved performance of a biomaterial-based cation exchanger for the adsorption of uranium(VI) from water and nuclear industry wastewater. *J. Environ. Radioact.*, 100: 250-257.
17. Anirudhan, T.S., L. Divya, P.S. Suchithra, 2009. Kinetic and equilibrium characterization of uranium(VI) adsorption onto carboxylate-functionalized poly(hydroxyethylmethacrylate) grafted lignocellulosics. *J. Environ. Manage.*, 90: 549-560.
18. Lloyd, J.R., J.C. Renshaw, 2005. Microbial transformations of radionuclides: fundamental mechanisms and biogeochemical implications. In: Sigel, A., Sigel, H., Sigel, R.K.O. (Eds.), *Metal Ions in Biological Systems: Biogeochemical Cycles of Elements*. CRC, pp: 205-240.
19. Bhatnagar, A., M. Sillanpaa, 2009. "Applications of chitin- and chitosan-derivatives for the detoxification of water and wastewater - A short review". *Advances in Colloid and Interface Science*, 152: 26-38.
20. Bhatnagar, A., A.K. Jain, 2005. A comparative adsorption study with different industrial wastes as adsorbents for the removal of cationic dyes from water. *J. Colloid Interface Sci.*, 28(1): 49-55.
21. Vijayaraghavan, K. and Yun, Yeung-Sang, 2008. Bacterial biosorbents and biosorption. *Biotechnology Advances*, 26: 266-291.
22. Castro, C.S., M.C. Guerreiro, M. Gonçalves,



- L.C.A. Oliveira, A.S. Anastácio, 2009. Activated carbon/iron oxide composites for the removal of atrazine from aqueous medium. *Bioresour. Technol.*, 164: 609-614.
23. Oliveira, L.C.A., R.V.R.A. Rios, R.J.D. Fabris, V. Garg, K. Sapag, R.M. Lago, 2002. Activated carbon/iron oxide magnetic composites for the adsorption of contaminants in water. *Carbon*, 40: 2177-2183.
24. Chang, Y.C., D.H. Chen, 2005. "Preparation and adsorption properties of monodisperse chitosan-bound Fe<sub>3</sub>O<sub>4</sub> magnetic nanoparticles for removal of Cu (II) ions". *J. Colloid Interf. Sci.*, 283: 446-451.
25. Chang, Y.C., S.W. Chang, D.H. Chen, 2006. "Magnetic chitosan nanoparticles: Studies on chitosan binding and adsorption of Co(II) ions". *React. Funct. Polym.*, 66(3): 335-341.
26. Ngarmkam, W., C. Sirisathitkul, C. Phalakornkule, 2010. Magnetic composite prepared from palm shell-based carbon and application for recovery of residual oil from POME. *J. Environ Management*, 265: 1-8.
27. Shen, Y.F., J. Tang, Z.H. Nie, Y.D. Wang, Y. Ren, L. Zuo, 2009. "Preparation and application of magnetic Fe<sub>3</sub>O<sub>4</sub> nanoparticles for wastewater purification".
28. Saifuddin, N., A.A. Nur Yasumira, 2010. "Microwave enhanced synthesis of chitosan-graft polyacrylamide molecular imprinting polymer (MIP) for selective extraction of antioxidants". *E-J. Chem.*, 7(4): 1362-1374.
29. Saifuddin, N., A.A. Nur Yasumira, S.F. Abdullah, 2011. Microwave Enhanced synthesis of Chitosan-Graft-Polyacrylamide molecular imprinting polymer for selective removal of 17 $\beta$ -estradiol at trace concentration. *Asian J. Biochem.*, 6(1): 38-54.
30. Saifuddin, N., S. Dinara, 2011. Pretreatment of palm oil mill effluent (POME) using magnetic chitosan. *E- J. Chem.*, 8(5): 324-331.
31. Gupta, A.K., Wells, S., 2004. Surface-modified superparamagnetic nanoparticles for drug delivery: preparation, characterization, and cytotoxicity studies. *IEEE Trans. Nanobiosci.* 3, 66-73.
32. Hu, L., Hach, D., Chaumont, D., Brachais, C.-H., Couvercelle, J.-P., 2008. One step grafting of monomethoxy poly(ethylene glycol) during synthesis of maghemite nanoparticles in aqueous medium. *Colloids Surf. A* 330, 1-7.
33. Ahmadi, R., Malek, M., Madaah Hosseini, H.R., Shokrgozar, M.A., Oghabian, M.A., Masoudi, A., Gu, N., Zhang, Y., 2011. Ultrasonic-assisted synthesis of magnetite based MRI contrast agent using cysteine as the biocapping coating. *Mater. Chem. Phys.* 131, 170-177.
34. Basti, H., Tahar, L.B., Smiri, L.S., Herbst, F., Vaulay, M.-J., Chau, F., Ammar, S., Benderbous, S., 2010. Catechol derivatives-coated Fe<sub>3</sub>O<sub>4</sub> and  $\gamma$ -Fe<sub>2</sub>O<sub>3</sub> nanoparticles as potential MRI contrast agents. *J. Colloid Interface Sci.* 341, 248-254.
35. American Cyanamid Company, 1989. *Cyanex 272, Technical Brochure.*
36. Kim, M., Jung, J., Lee, J., Na, K., Park, S., Hyun, J., 2010. Amphiphilic comblike polymers enhance the colloidal stability of Fe<sub>3</sub>O<sub>4</sub> nanoparticles. *Colloids Surf. B* 76, 236-240.
37. Wang, J.L., 2002. Biosorption of copper(II) by chemically modified biomass of *Saccharomyces cerevisiae*. *Process Biochem.*, 37: 847-50.
38. Wang, J.L. and C. Chen, 2009. Review: Biosorbents for heavy metals removal and their future. *Biotechnology Adv.*, 27: 195-226.
39. Wang, J.L., C. Chen, 2006. Biosorption of heavy metals by *Saccharomyces cerevisiae*: A review. *Biotechnol Adv.*, 24: 427-51.
40. Wang Guanghui, Liu Jinsheng, Wang Xuegang, Xie Zhiying, Deng Nansheng, 2009. Adsorption of uranium (VI) from aqueous solution onto cross-linked chitosan. *J. Hazardous Materials*, 168: 1053-1058.
41. Kutahyal Ceren, M. Eral., 2004. "Selective adsorption of uranium from aqueous solutions using activated carbon prepared from charcoal by chemical activation". *Sep. Purif. Technol.*, 40: 109-114.
42. Hudson, M.J., Z. Matejka, 1989. Extraction of copper by selective ion-exchangers with pendent ethyleneimine groups—investigation of active states. *Sep. Sci. Technol.*, 24: 1417-1426.
43. Erdal, U.G.G., B.D. Emir, E. Öztürkb, 2009. Preparation and characterization of poly(ethylene glycol) methacrylate (PEGMA)-co-vinylimidazole (VI) microspheres to use in heavy metal removal. *J. Hazard. Mater.*, 162: 1073-1080.
44. X. Han, W. Wang, X. Ma, *Chemical Engineering Journal* 171 (2011) 1.
45. M. Ugurlu, *Microporous and Mesoporous*



- Materials 119 (2009) 276.
46. R. Katal, M.V. Sefti, M. Jafari, A.H. Saeedi, M. Sharifian, *Journal of Industrial and Engineering Chemistry* 18 (1) (2012) 230.
47. B.K. Nandi, A. Goswami, M.K. Purkait, *Applied Clay Science* 42 (2009) 583.
48. Q.d. Qin, J. Ma, K. Liu, *Journal of Hazardous Materials* 162 (2009) 133.
49. S. Lagergren, *Handlingar* 24 (1898) 1.
50. Y. Sag, Y. Aktay, *Biochemical Engineering Journal* 12 (2002) 143.
51. A.K. Bhattacharya, T.K. Naiya, S.N. Mandal, S.K. Das, *Chemical Engineering Journal* 137 (2008) 529.
52. Y.A. Aydin, N.D. Aksoy, *Chemical Engineering Journal* 151 (2009) 188.
53. R. Katal, E. Hasani, M. Farnam, M. Sharfizadeh, M.A. Ghayyam, *Journal of Chemical and Engineering Data* 57 (2012) 374.
54. S.J. Azizian, *Journal of Colloid and Interface Science* 276 (2004) 47.
55. M. Omraei, H. Esfandian, R. Katal, M. Ghorbani, *Desalination* 271 (1-3) (2011) 248.
56. W.H. Cheung, Y.S. Szeto, G. McKay, *Biore-source Technology* 98 (2007) 2897.
57. W.J. Morris, C.I. Weber, *Journal of the Sanitary Engineering Division, ASCE* 89 (1963) 31.
58. X.Y. Yang, S.R. Otto, A.D. Bushra, *Journal of Chemical Engineering* 94 (2003) 199.
59. X.Y. Yang, A.D. Bushra, *Journal of Chemical Engineering* 83 (2001) 15.
60. Mellash, A., S. Chegrouche, 1997. The removal of zinc from aqueous solution by natural Bentonite. *Water Res.*, 31: 621-629.
- P. Manouchehri; S. A.Milani; H. Abolghasemi, 2021, Use of response surface methodology for optimizing process parameters of thorium adsorption on amino-functionalized titanosilicate nanoparticles, *The Journal of Nuclear Science and Technology*, Volume 42, Issue 1, April 2021, Pages 57-66